EVAPORATION FROM SIMULATED SOIL PORES: EFFECTS OF WETTABILITY, LIQUID ISLANDS, AND BREAKUP

Partha Pratim Chakraborty[1], Ryan Huber[1], Xi Chen[1,2], Melanie M. Derby[1*]

[1]Kansas State University, Manhattan, KS 66506, USA
[2]Intel Corporation, Hillsboro, OR, USA 97124

[*]derbym@ksu.edu

Abstract

Two-thirds of worldwide water withdrawals are for agriculture; this represents a key challenge in the food-energy-water nexus. In the U.S. Central High Plains, the Ogallala aquifer – the primary water source for agriculture – is depleting. Reducing water evaporation from soil provides an opportunity to decrease irrigation, thus conserving water resources. In this study, evaporation phenomena of 4-μL sessile water droplets were analyzed from a simulated soil pore created with 2.38-mm hydrophilic glass and hydrophobic Teflon beads. The experiments were conducted at 22ºC and 60% relative humidity. Two geometries were studied: symmetric (i.e., center-to-center spacing between the beads of 3.1 mm) and asymmetric (i.e., center-to-center spacings of 2.7 mm and 2.8 mm). Evaporation phenomena were recorded using a high-speed camera and evaporation times were recorded. Evaporation was faster from the hydrophilic pore (e.g., 34 minutes) compared to the hydrophobic pore (e.g., 42 minutes) in the symmetric configuration, due in part to greater air-water contact areas. Spacing between the beads affected evaporation, as evaporation rates to completely evaporation the droplet were slower for hydrophilic (e.g., 44 minutes) and hydrophobic (e.g., 56 minutes) pores in the asymmetric configuration. The formation of liquid island, projected area, liquid island contact angles, volume and rupture strength of droplet were analyzed for all four combinations. The droplet retained its initial projected area, wetted length and volume for a certain

time during evaporation from Teflon pores (e.g., 5–10 minutes), while these parameters decreased simultaneously during evaporation from glass pores.

KEY WORDS: Food-Energy-Water Nexus, liquid bridges, mixed wettability, hydrophobicity

NOMENCLATURE

a	Beads separation distance [mm]
b	$\sqrt{(1+2\tilde{V})^{\frac{1}{3}}/\pi(1+\theta/2)^2}$
CA	Contact Angle
d_p	Beads diameter [mm]
$d_{sp/sp}$	Immersion distance [mm]
F, F_{cap}	Resulting total force/ capillary force [μN]
RH	Relative Humidity [%]
R_1, R_2	Principal radii of curvature [mm]
S^+	Dimensionless separation distance $[\frac{a}{2\sqrt{\frac{V}{R}}}]$
$\widetilde{W}$	Dimensionless rupture energy $[\frac{W}{\sigma r^2}]$
V	Volume of liquid island [μL]
$\tilde{V}$	Dimensionless bridge volume [V/R]

Greek Symbols

α	Embracing angle [radian]
β	Half filling angle [radian]
γ	Surface tension of water [mN/m]
δ	Contact angle [radian]

Subscripts/Superscripts

1,2	Corresponding to first and second measuring segment
cap	Capillary force
+	Non-dimensional parameter
v	vapor

1. INTRODUCTION AND LITERATURE REVIEW

Food, energy and water systems are inter-connected and new innovations are required to feed the growing global population [e.g., estimate of 9.8 billion people by 2050 (United Nations, 2017)] without a significant increase in arable lands (Alexandratos and Bruinsma, 2012) . Agriculture is responsible for two-thirds of water withdrawals worldwide (Oki and Kanae, 2006). Surface-level water sources such as ponds, rivers, and reservoirs can serve as irrigation sources but are susceptible to drought (Hornbeck and Keskin, 2014). In much of the Central High Plains, the Ogallala aquifer is the primary source of water and since the annual average rainfall in western Kansas is only 12-14 inches. As a result, there are 1.5 million acres of irrigated lands in southwestern Kansas and the Ogallala aquifer provides 90% of the water for irrigation in these lands (Steward et al., 2013; Wise, 2015). The diminishing trend of the Ogallala water level and insufficient recharge rates for aquifer account for strong need of sustainable water in the intersection of food and energy (Butler et al., 2013; Gleeson et al., 2012; Steward and Allen, 2016; Steward et al., 2013). Reduction in soil evaporation rates can reduce irrigation rates; this research proposes to reduce soil water evaporation by altering soil hydrophobicity.

Previous research demonstrated that evaporation from hydrophobic soil or simulated soils can be 50-65% lower than evaporation from hydrophilic soils (Bachmann et al., 2001; Davis et al., 2009, 2014; Shokri et al., 2008). Shokri et al. (2008) studied evaporation from hydrophilic sand columns in the presence of hydrophobic layers at 25.9˚C and 22% RH over 30 days. Four different combinations were investigated, which included varying the position and thickness of hydrophobic layer. The largest evaporative mass loss was observed from the 25-mm-deep hydrophilic column and the lowest evaporative losses were observed in the 25-mm-deep hydrophobic column and 18-mm hydrophilic/7-mm hydrophobic column.

Soil contact angles can be challenging to measure due to a lack of sample cleanliness and inherent surface roughness; many naturally-occurring minerals are hydrophilic, but soils can be hydrophobic in part due to the presence of organic materials. Using the sessile droplet method with water, the following contact angles were measured on common soil minerals, 22.8º (goethite), 27.8º (Ca-kaolinate), 43.3º (Ca-illite), 46.9º (hematite) 55.7º (Ca-smectite) (Shang et al., 2008) as well as contact angles between 59–68º on Ottawa sand (Keatts et al., 2018). Bachmann et al. (2003) studied contact angles on 17 different soils using multiple methods. The sessile drop method yielded contact angles of water on soil samples from 0-135º based on soil composition.

Researchers have studied evaporation of sessile water droplets from hydrophilic and hydrophobic surfaces other than soil. Concentration gradients [i.e., humidity (Hu and Larson, 2002)], droplet pinning/contact line dynamics ((Birdi and Vu, 1993; Deegan et al., 2000; Hu and Larson, 2002; Nguyen et al., 2012; Orejon et al., 2011), and droplet contact areas and contact angles (Birdi et al., 1989; Nguyen, et al., 2012; Orejon, et al., 2011) were shown to be important parameters governing the evaporative process. It was noted that evaporation of sessile water droplet is a complex phenomenon and most papers described this as a quasi-static process.

Evaporation is motivated by a concentration difference and, according to the ideal gas law, the concentration equals the vapor pressure of liquid at the given temperature or the difference between saturation and relative humidity (Erbil, 2012).

Evaporation of water droplets was investigated by Birdi and Vu (1993) on flat glass (CA 41^{o}) and Teflon (CA 108^{o}) surfaces. Evaporation was generally linear with respect to time for the hydrophilic case and the drop was primarily pinned (i.e., stationary air-water-solid contact line). Therefore, contact angles decreased. For the hydrophobic case, evaporation was non-linear, and the hydrophobic contact angle was maintained while the droplet area in contact with the surface decreased, resulting in a moving air-water-solid contact line. Similarly, air-fluid-solid contact lines were studied during the evaporation of water on glass (CA 28^{o}), silicon (CA 57^{o}), Cytop (CA 108^{o}) and Teflon (CA 114^{o}), and other fluid-surface combinations (Orejon et al., 2011). On hydrophilic surfaces, the contact line was pinned initially (e.g., 40% of water droplet lifetime on silicon), whereas on hydrophobic surfaces, there was a slight, initial decrease in contact angle and then the contact angle remained steady until the final evaporation stage. Evaporation of sessile pinned water droplets was investigated. The droplet was pinned for 90-95% of evaporation time and the difference in relative humidity between saturated water droplet and air-water mixture was the driving potential (Hu and Larson, 2002). It was noted that during evaporation, droplets on hydrophilic surfaces were initially pinned; subsequently, the contact angle was constant and wetted area changed. The time required to completely evaporate the droplet was higher for droplets on hydrophobic surfaces than on hydrophilic surfaces (Nguyen et al.,2012).

Fewer studies investigated non-spherical droplet evaporation (Saenz et al.,2017) and effect of droplet size on evaporation (Borodulin and Nizovtsev, 2017). Saenz et al. (2017) studied sessile

1–7 μL, pinned, non-spherical droplets. They noted that evaporation was not merely a function of droplet-air interface and was affected by droplet shape and curvature. According to Borodulin and Nizovtsev (2017), droplet shape impacts evaporation, as the accommodation coefficient has more significance on evaporation for small droplet than larger one. Surface geometry can also affect apparent contact angles. Droplets on nano-pillared structures can have apparent contact angles different than bulk values, particularly when the height and spacing between the nano-pillars are increased (Suzuki and Ueno, 2017; Haque et al.,2018). Suzuki and Ueno (2017) studied 2-μL water droplets on 33 patterned polymethyl methacrylate (PMMA) samples. With the same bulk material, contact angles of approximately 80–120^{o} were observed, and the differences were attributed to the impacts of interfacial tension and pinning.

Seminal work on soil evaporation mechanisms noted that evaporation rates in partially dried out soils were 1.5-5 times that predicted by diffusion. Increased evaporation rates were attributed to the formation of liquid islands between soil particles. Condensation and evaporation across liquid bridges increased evaporation compared to vapor diffusion and this phenomenon was termed “enhanced vapor diffusion”; therefore, liquid bridges are an important topic of study(Philip and De Vries, 1957; De Vries, 1958). Previous research were conducted on liquid bridges, or liquid islands, formed between two particles (Pietsch and Rumpf, 1967; Fairbrother and Simons, 1998; Weigert and Ripperger, 1999; Farmer and Bird, 2015; Zhu et al., 2007; Lian et al., 1993). Pietsch and Rumph (1967) derived an equation to measure the volume of liquid bridge with two radius of curvatures and contact angles. The analysis was conducted for imperfect wetting. Fairbrother and Simons (1998) derived an equation for the half liquid bridge created between uneven spheres; the half liquid bridge results when the bridge is divided at its thinnest part. Weigert and Ripperger (1999) compared previous works related to the geometry of liquid bridge and also analyzed the

volume of half and full liquid bridge. Farmer and Bird (2015) used surface evolver and numerical speculations to define the parameters of asymmetric liquid bridge between contacting spheres.

Analysis of rupture strength is also an important parameter to analyze the properties of liquid bridges or liquid islands. For the liquid islands, rupture strength equations were derived with respect to capillary force (Willett et al., 2000; Gladkyy and Schwarze, 2014; Lambert et al., 2008; De Bisschop and Rigole, 1982; Pitois et al., 2001; Simons et al.1994), contact angle and half filling angle (Weigert and Ripperger, 1999), and embracing angle (Rabinovich et al., 2005). Willett et al. (2000) proposed two methods (i.e., full model and reduced model) to analyze the rupture strength. In the first approach, an equation was derived with numerical data from integration of Young-Laplace equation. In the second method, the capillary force of liquid bridge between two similar spheres was evaluated.

The research objectives of this paper are to observe evaporation of sessile water droplets on spherical hydrophilic and hydrophobic beads. Analyses of this process include contact angle dynamics, projected area, liquid island formation, and prediction of rupture during evaporation.

2. EXPERIMENTAL METHODS

2.1 Experimental Apparatus

Evaporation of sessile deionized water droplets were observed from simulated soil pores (Figure 1). Soil pores were created with hydrophilic borosilicate glass and hydrophobic PTFE (polytetrafluoroethylene) beads. Four different combinations of 2.38-mm-diameter beads were used to determine the effects of wettability and beads distance: two wettabilities (i.e., all hydrophilic or all hydrophobic) and two distances (i.e., same center-to-center distances of beads, a=3.1 mm, and center-to-center distances of beads are asymmetric, a=2.7 mm and b =2.8 mm), as shown in Figure 2. A fixture was created via additive manufacturing and was used to hold the

beads in the desired location; the water droplet was only in contact with the beads and did not touch the fixture. A 4-μL water droplet was placed in the center of the pore created by three beads using a 0.2-2 μL pipette (Fisherbrand ELite). Food coloring (i.e. dye, 2-3% of volume) was added to the deionized water to provide better contrast in imaging.

Experiments were conducted in a quiescent environment at 22 ºC and 60% RH. An LED lamp (WD-8W) with magnetic base was used to illuminate the sample. The evaporation phenomena were captured using a high-speed camera (Fastec IL3) with a magnification of 5× and evaporation times were determined from videos recorded using Fastmotion. The captured files were processed and analyzed later using PFV (Photron FASTCAM Viewer), Active-presenter, and SolidWorks 2018.

2.2 Static Contact Angles

Static contact angles of water droplets on glass and Teflon beads were measured using a goniometer and high speed camera (Figure 3). Contact angles of 8-μL water droplets on flat glass and Teflon surfaces were ~20º and 110º, respectively (Figure 3a and b). Flat, glass contact angles were similar to several minerals found in soil [e.g., 22.8º (goethite) and 27.8º (Ca-kaolinate), (Shang et al., 2008)], whereas contact angles on the flat, Teflon surface were similar to several contact angles from real soils [e.g., 95º, 109º, and 129º, (Bachmann et al. (2003)]. As shown in Figure 3c and 3d, hydrophilic and hydrophobic contact angles similar to the flat plates were observed from a, 8-μL water droplet placed on a glass or Teflon pore on with a center-to-center spacing of approximately one bead diameter (i.e., the beads were touching). As the bead spacing increased to the asymmetric spacing, contact angles reduced due to the stretching of the 4-μL droplet (Figure 3e and f). Suzuki and Ueno (2017) and Haque et al. (2018) noted differences in

apparent contact angles (e.g., 80–120º for water on PMMA surfaces) based on droplet pinning and surface texture.

3. RESULTS AND DISCUSSION

As a brief overview of the results and discussion section follows. Evaporation dynamics of sessile water droplets from simulated soil pores created with three hydrophilic glass and hydrophobic Teflon beads in two different combinations (i.e. symmetric and asymmetric) were investigated. After breakup of the droplet suspended between three beads, the formation of liquid islands along with the predictions of liquid island breakup were evaluated. During evaporation, parameters such as projected area, wetted length, contact angle dynamics of liquid island, deformation of volume and analysis of rupture strength of liquid island were evaluated for both combinations (i.e. symmetric and asymmetric).

3.1 Evaporation Time and Projected Area

Sessile water droplets were evaporated and projected areas (i.e. areas captured from top view projection) were observed and analyzed from the four pores created by hydrophilic and hydrophobic beads. The evaporation phenomena of sessile water droplet and liquid island formed between two beads from different soil pores, including the deformation of evaporating water droplets from glass and Teflon pores (symmetric combination i.e. center-to-center spacing~ 3.1 mm) are shown in Figure 4(a, b) and Figure 5(a, b). The average time to evaporate 4-µL water droplets is 34 and 42 minutes for glass and Teflon pores (symmetric combination), respectively (Table 1). That means the evaporation time ratio of Teflon to glass is approximately 1.2. In glass beads, the droplet stretched and air-water contact areas are larger, resulting in shorter total evaporation times. Figure 4(c, d) and Figure 5(c, d) show the evaporation phenomena from a simulated soil pore created with three glass and three Teflon beads where the beads distances are

smaller (asymmetric). As the beads' separation distances are smaller, the surface area for the water droplet are also lower, thus creating smaller air-water contact area. Therefore, the evaporation rates are slower than the previous cases. For glass beads, it took on average 42 minutes and from Teflon beads it took approximately 55 minutes to evaporate 4-μL sessile water droplet (i.e. ~1.3 evaporation time ratio of Teflon to glass).

The overall experiments and evaporation dynamics were captured using a high-speed camera and top view images were used to analyze the change of projected areas and liquid island contact angles. Images were analyzed in SolidWorks 2018. Figure 4 represents the change of projected area of whole droplet during evaporation for all four cases. The initial projected area is higher for the glass pores compared to the Teflon pores of the same spacing, symmetric [i.e. 3.95 mm^2 for glass and 3.54 mm^2 for Teflon (ratio of 1.1)] and asymmetric [3.53 mm^2 for glass and 2.76 mm^2 for Teflon (ratio of 1.3)]. In glass pores, the initial projected area is higher and it tends to decrease during evaporation; for the Teflon beads, the droplet retains its initial shape for approximately 5–10 minutes.

3.2 Liquid Island Formation

As the droplet evaporation continues, the whole droplet breaks up and forms liquid islands in order to minimize surface energy. Figure 4 represents the change of projected area of liquid islands during evaporation. Similarly, the reduction rate of projected area from glass surface is higher than the Teflon. From glass surface, the area decreases in a continuous manner which demonstrates higher evaporation rate and wettability of glass surface. In the symmetric combination for Teflon, the liquid island also has a tendency to sustain its initial formation and then it starts to decrease significantly after 42 minutes. However, for the lower distance,

asymmetric combination, the Teflon surface decreases in a continuous pattern. Lower distance and higher time to form liquid islands in that case could contribute to such behavior.

During evaporation of 4-μL droplets of water, the whole-droplet breakup and formation of liquid bridge were observed and analyzed for the four cases presented in Figure 6. Table 2 shows the average time of liquid island formation between two beads for all four combinations. It can be seen that, between the two spacings (i.e., symmetric and asymmetric) tested, it takes more time to form a liquid island when the bead-to-bead distance is smaller. Between glass and Teflon beads, liquid island formation times were higher for Teflon beads (e.g., 19 minutes for glass and 28 minutes for Teflon when a=3.1 mm).

As shown in Figure 6, liquid islands are formed between two beads in all four combinations, and the radii of liquid islands decreased from both sides. The formation of liquid islands during evaporation played a vital role in the pioneering work on soil evaporation (Philip and De Vries, 1957; De Vries, 1958), which analyzed the movement of water through liquid islands under a temperature gradient and different radii due to condensation on one side of the liquid island and evaporation on the opposing side. In this research, the experiments were conducted in a quiescent atmosphere without a temperature gradient or vapor flux. Therefore, both sides of the liquid island will experience evaporation equally, as reflected by the symmetric liquid islands' radii observed in these experiments.

Figure 6 shows the evolution of the radius of curvature of liquid islands for all four combinations. Radii of curvature were obtained using SolidWorks 2018 for images recorded at two-minute time intervals. For the symmetric spacing, the radius decreases at a faster rate in glass than Teflon. In Teflon, the island retains its initial position for a certain time period (e.g. ~ 4 minutes) and then it starts to decrease. However, in the asymmetric combination, the radius

decreases similarly from both glass and Teflon surface. It takes more time (e.g. ~ 35 minutes in glass and ~43 minutes in Teflon) to form liquid island in the asymmetric combination and the liquid bridge lifespan is briefer. The liquid island snaps off immediately after 30 minutes for glass and 44 minutes for Teflon in symmetric combination and, for the assymetric combination, it snaps off after 42 minutes and 54 minutes for glass and Teflon, respectively.

3.4 Wetted Length

To understand the droplet geometries and evaporation phenomena, analyses of wetted length (i.e. the perimeter of water contact line with beads, as indicated in Figure 7) of droplet during evaporation were conducted twice – first, from the beginning until the formation of liquid island and second from the liquid island until the end of evaporation. Figure 7 and Figure 8 represent the deformation of wetted length before and after formation of liquid islands, respectively. The initial wetted length for asymmetric combination (i.e. a=~2.7 mm, b=~2.8 mm) is highest for Teflon (5.8 mm) and the lowest initial wetted length were found in symmetric Teflon (5.34 mm) though the differences among the initial wetted lengths are almost the same for all four cases (Figure 7). As the droplet continuously deforms during evaporation, the change of liquid island contact angles and other parameters might have some effect on deformation of wetted length. Some irregularities can be seen from Figure 7 for all the four cases, where instead of decreasing, the wetted length tends to increase (e.g. 6-8 minutes and after 20 minutes). If comparison is made between two Teflon models (symmetric and asymmetric), it can be seen that, the asymmetric one is following decreasing trend to sustain its initial wetted length, while in the other combination, the wetted length decreases without some irregularities. This phenomenon could be influenced by the increased distance between the beads which causes stretching. For the glass beads, the wetted

length decreases as usually while there are some increases at certain points. These increasing behavior can be influenced by continuous change in inside and outside geometry of the droplet.

Figure 8 represents the wetted length change during evaporation of liquid island for all four cases. Asymmetric combination where the distances are smaller than the symmetric one, takes more time to form liquid island and they do not last long. The initial wetted lengths of both symmetric cases are greater than the asymmetric one and for all the four combinations the wetted lengths decrease after formation of liquid islands until the last state of evaporation.

3.5 Volume and Contact Angles of Liquid Islands

In the theories proposed by Philip and De Vries (1957), liquid islands were shown to be very important during evaporation from soils at partial dry out. Therefore, due to the importance of liquid islands, the contact angle dynamics and volume of liquid islands between two spheres were analyzed. The bridge profile is approximated as circular arc and imperfect wetting (i.e. contact angle is not equal to zero) has been assumed. Figure 9 represents the liquid island and its different parameters of a liquid island formed between two beads. Pietsch and Rumph (1967) gave the following expression of liquid island volume for imperfect wetting,

$$\frac{V}{2\pi} = (R_1^2 + b^2)R_1 \cos(\beta + \delta) - \frac{R_1^3 cos^3(\beta + \delta)}{3} - b\left[R_1^2 cos(\beta + \delta)\sin(\beta + \delta) + R_1^2\left(\frac{\pi}{2} - \beta - \delta\right)\right] - \frac{1}{24}d_p^3\,(2 + cos\beta)(1 - cos\beta)^2 \quad (1)$$

including the following parameters,

$$R_1 = \frac{d_p(1 - cos\beta) + a}{2\cos(\beta + \delta)} \quad (2)$$

$$R_2 = \frac{d_p}{2} sin\beta + R_1[\sin(\beta + \delta) - 1] \quad (3)$$

$$b = R_1 + R_2 \quad (4)$$

where beads diameter is *dp*, beads separation distance *a*, the principal radii of curvature R_1 and R_2, half filling angle β, contact angle δ and *b* is the summation of two principal radii of curvature *R1* and *R2*. With this model, liquid island volumes were calculated and contact angles were measured by using SolidWorks 2018. After breakup of the whole droplet, two-minute time intervals were given for the liquid island to stabilize and then liquid island contact angles and volume were measured.

Figure 10 demonstrates the evolution of liquid island volume. The initial volume of liquid island in the glass pores [i.e., 1.71-µL (*a*=~3.1 mm and 0.43-µL (*a*=~2.8 and *b*=~2.7 mm)] are larger than Teflon [i.e., 1.54-µL (*a*=~3.1 mm and 0.41-µL (*a*=~2.8 and *b*=~2.7 mm)] (equation 1) and it decreases till the final breakup happens. From glass surface, the volume decreases at a faster rate than Teflon. Due to hydrophilic properties and wetting characteristics of glass, faster rate of volume reduction can be justified.

Variations of liquid island contact angles with volume can be observed (Figure 11**)**. For all four combinations, the liquid island contact angle decreased with decreasing volume. Initial contact angle in Teflon surface [i.e., 15.91º (*a*=~3.1 mm) and 22.08º (*a*=~2.8 and *b*=~2.7 mm)] was found to be slightly higher than the glass combinations [i.e., 15.23º (*a*=~3.1 mm) and 15.47º (*a*=~2.8 and *b*=~2.7 mm)], though the difference is small. Interestingly, in the combination where the distance was lower, the contact angles were greater due to reduced droplet stretching. From the

plot, it can be seen that, the contact angles decreased in an almost similar pattern though from Teflon surface, the contact angle retained its initial position for a while and then it decreased. From the glass pores, the contact angles decreased more rapidly than the Teflon. Typically, due to hydrophilic properties, in glass the contact angle should vary/ decrease at a faster rate than Teflon and from Figure 11, this theory can be verified.

3.5 Uncertainty Analysis

In these experiments, the same bead combinations were repeated four times while atmospheric conditions and other parameters were also kept constant. The images were captured using a high-speed camera and later they were processed with SolidWorks 2018. Two parameters, namely liquid island contact angle and radius of curvature, were chosen to analyze uncertainty and they were measured four times with SolidWorks using same pixel size. Some uncertainty analysis has been shown in Table 3. The contact angles and principal radii of curvature of liquid island in glass surface (a=~3.1 mm) have been measured four times. For the contact angle analysis, the highest uncertainty level was found 1.67% and for the principal radii of curvature they were 1.9% and 2.2% respectively. All the data points are within the range of ±2.5%.

3.6 Capillary Force/ Rupture Strength

If the surface free energy of two islands is smaller than that of the liquid island, snap-off is thermodynamically favored and rupture will occur. Previous researchers analyzed capillary force/rupture strength of liquid islands formed between two identical spheres (Zhu, et al., 2007; Lian, et al., 1993; Pitois, et al., 2001). Zhu et al. (2007) evaluated force of the liquid island as Capillary Bridge Model (CBM) and according to their theory, CBM method is easier to determine

bridge volume based on separation distance. In the study of Lian et al. (1993), it was mentioned that, the total capillary attractive force between two particles is caused by a surface tension component and hydrostatic pressure of the bulk. Pitois et al. (Pitois, et al., 2001) used a circular approximation for the bridge profile and obtained a simplified expression for the capillary force which when integrated throughout the separation distance, led to expression for the dimensionless rupture energy,

$$\widetilde{W} = 2\pi\, cos\delta\, [\left(1 + \frac{\delta}{2}\right)(1 - A)\tilde{V}^{\frac{1}{3}} + \sqrt{\frac{2\tilde{V}}{n}}] \tag{5}$$

where, $A = \sqrt{\left(1 + 2\tilde{V}\right)^{\frac{1}{3}}/\pi(1 + \delta/2)^2}$ and δ is the contact angle in radians.

The rupture energy model proposed by Simons et al. (1994) is derived by the integration of total liquid bridge force, which is written as

$$F = \pi\gamma R\, (1 + Xtan\beta - Xsec\beta)\frac{Xtan\beta}{Xsec\beta - 1}. \tag{6}$$

Weigert and Ripperger (1999) evaluated empirical equations to calculate V and half filing angle β from the bulk liquid saturation. The expression of F_{cap} according to their theory is

$$F_{cap} = \frac{\pi}{4}\,(2R)^2 sin^2\beta.p_k + \gamma\pi 2Rsin\beta\,\sin(\beta + \delta) \tag{7}$$

where, the first term F_p is the hydrostatic pressure component and the second term F_γ is the liquid surface tension contribution.

Willet et al. (2000) proposed a less complex CBM for equal sized particles or beads $R_i = R_j = R$. The following equation provides a closed approximation of F_{cap} between equal sized particles.

$$F_{cap} = \frac{2\pi R\gamma cos\delta}{1 + 2.1(S^+) + 10\ (S^+)^2} \tag{8}$$

where,

$$S^+ = \frac{a}{2\sqrt{\frac{V}{R}}}. \tag{9}$$

Rabinovich et al. (2005) proposed the following expression which is based on combined experimental and numerical analysis. First of all, the "embracing angle", α is evaluated:

$$\alpha = \sqrt{\frac{a}{R}.(-1 + \sqrt{1 + \frac{2V}{\pi R a^2}})} \tag{10}$$

Then the immersion distance $d_{sp/sp}$ was evaluated using the following expression,

$$d_{sp/sp} = \frac{a}{2}[-1 + \sqrt{1 + \frac{2V}{\pi R a^2}}]. \tag{11}$$

Finally, F_{cap} is predicted with:

$$F_{cap} = -\frac{2\pi R\gamma cos\delta}{1 + \left[\frac{a}{2d_{\frac{sp}{sp}}}\right]} - 2\pi\gamma R sin\alpha \sin(\delta + \alpha) \tag{12}$$

Lambert et al. (2008) modified the Rabinovich et al. (2005) model and deduced a new equation,

$$F_{cap} = -\frac{2\pi R\gamma cos\delta}{1 + \left[\frac{a}{2d_{\frac{sp}{sp}}}\right]}. \tag{13}$$

In this research, the Willet et al. (2000), Rabinovich et al. (2005) and Lambert et al. (2008) models have been used to determine the capillary/rupture strength of the liquid island. The rupture strength was derived in μN, where the distance between the beads were 0.8 mm for the

first and 0.35 mm for second combination, beads diameter $d_{p,}$ was 2.38 mm, surface tension of water, γ was 72.75 mN/m, principal radii of curvature R_1 and R_2 were in mm, half filling angle β and contact angle δ were in degree and volumes, v were in µL. For first combination, where the distance was larger, rupture strength was measured at a three minutes' time interval and for the second combination, two minutes' time interval were considered after formation of liquid island. R_1 and R_2, β and δ were measured continuously using SolidWorks 2018 from the processed images. Volume v was derived using equation (1) at certain time frames and Eqs. (8,12,13) were used to measure rupture strength/ capillary force according to Willet et al. (2000), Rabinovich et al. (2005) and Lambert's (2008) models, respectively.

Figure 12 shows the variation of rupture strength/capillary force with time for all four combinations. From the graph, it can be seen that, according to the three models [i.e. Willet et al. (2000), Rabinovich et al. (2005) and Lambert et al. (2008)], the predicted rupture strength/capillary forces are nearly the same. There were slight differences between the Willet et al. (2000) model and the other two, but the Rabinovich et al. (2005) and Lambert et al. (2008) models almost overlapped in every single data points. From the plot, it can be seen that, the initial force after formation of liquid island in Teflon [~177-µN (a=~3.1 mm) and ~215-µN (a=~2.8 and b=~2.7 mm)] is larger than glass [~170- µN (a=~3.1 mm) and 212- µN (a=~2.8 and b=~2.7 mm)] and then decreased slowly with time.

For both combinations, the initial rupture strengths were found greater when the distance was smaller (i.e. asymmetric combination). This phenomenon can be verified by the research of Gladky and Schwarze (2014). In their work, it was seen that, the rupture strength continuously decreased with increasing particle distance i.e. larger rupture strength with smaller distance. From Figure 12, similarities can be found between this and Gladky's (2014) work. Similar to Gladky's (2014) work,

the rupture strength was found larger when the distance was smaller (i.e. asymmetric combination) in this experiment.

In that study, rupture strength of liquid islands were evaluated by applying the Willet et al. (2000), Rabinovich et al. (2005) and Lambert et al. (2008) models with dimethylsiloxane as a reference fluid. Rupture strengths were derived in μN and comparison among three models were drawn. The distances between the beads were changed continuously and the effect of beads distance on rupture strength was evaluated. According to the data of Gladky et al. (2014), the Willet and Rabinovich's model almost overlapped and the Lambert's model was excluded as it is almost similar to Rabinovich's (2005) model from the plot. Weigert's (1999) model was also evaluated using equation (6), though it had a larger difference than the other two.

In hydrophilic surface for both combination, the rupture strength/ capillary force was found to reduce at a faster rate than the hydrophobic one. The final force, just before the breakup of the liquid island were found almost similar for glass and Teflon when the distance was larger (~0.52-μN and ~0.57-μN). However, in the second combination (a=~2.8mm, b=~2.7 mm), the final rupture strength was found larger in glass (~13-μN) than Teflon (~2-μN). In Teflon, the liquid island formed later than glass and the final size of liquid island before breakup was too small. That could be the reason of smaller rupture strength before final breakup. Most significantly, during evaporation, water tends to move from higher energy position to lower energy. In this experiment, from Figure 12, it can be seen how rupture strengths were decreasing and the strength/ force reached its lowest value before final breakup.

4. CONCLUSIONS

In this paper, evaporation of sessile 4-μL water droplets were observed and analyzed from hydrophilic glass and hydrophobic Teflon pores. A simulated soil pore was created using

three beads (hydrophilic and hydrophobic) and according to the beads distances symmetric and asymmetric combinations were made to analyze evaporation phenomena. Certain parameters like evaporation time, liquid island formation, projected areas, wetted length, change in volume, variation of contact angle and rupture strength were analyzed and compared among all four combinations.

- Evaporation rates were faster in glass pores than Teflon for both spacings investigated, although the symmetric combination experienced higher evaporation rates (i.e., shorter evaporation times).
- Liquid islands formed earlier (~19 minutes for glass and ~28 minutes for Teflon) and ruptured sooner in symmetric combination.
- Projected areas, wetted length and volume retained initial values during evaporation from Teflon for approximately 5–10 minutes, while they decreased simultaneously during evaporation from glass.
- Rupture strength was found to be higher when distance was lower.

This research indicates that contact angle dynamics affect evaporation from simulated soil surfaces, thereby delaying evaporation from hydrophobic pores. This phenomenon can, in turn, affect the soil water availability in the field, particularly when fallow. Future work is needed to scale up from pore-scale to larger scales in order to analyze the impacts of liquid capillary transport and these altered liquid islands from hydrophobicity on evaporation in soils, as well as the impacts of increased soil water availability on irrigation and yields.

5. ACKNOWLEDGEMENTS

The authors sincerely acknowledge the grant NSF CBET 165141 for financial support.

REFERENCES

Alexandratos, N., and Bruinsma, J., *World agriculture towards 2030/2050: the 2012 revision*, 2012

Bachmann, J., Horton, R., and Van Der Ploeg, R. R., Isothermal and nonisothermal evaporation from four sandy soils of different water repellency, *Soil Science Society of America Journal*, vol. 65, no. 6, pp. 1599-1607, 2001

Bachmann, J., Woche, S. K., Goebel, M. O., Kirkham, M. B., and Horton, R., Extended methodology for determining wetting properties of porous media, *Water Resources Research,* vol. 39, no. 12, pp. SBH111-SBH1114, 2003

Birdi, K. S., Vu, D. T., and Winter, A., A study of the evaporation rates of small water drops placed on a solid surfac, *Journal of Physical Chemistry,* vol. 93, no. 9, pp. 3702-3703, 1989

Birdi, K. S., and Vu, D. T., Wettability and the evaporation rates of fluids from solid surfaces, *Journal of Adhesion Science and Technology,* vol. 7, no. 6, pp. 485-493, 1993

Borodulin, V., and Nizovtsev, M., Effect of the size of droplets on evaporation, *Interfacial Phenomena and Heat Transfer,* vol. 5, no. 4, pp. 251-261, 2017

Butler, J. J., Stotler, R. L., Whittemore, D. O., and Reboulet, E. C, Interpretation of Water Level Changes in the High Plains Aquifer in Western Kansas, *Groundwater,* vol. 51, no. 2, pp. 180-190, 2013

Cary, J. W., Onsager's relation and the non-isothermal diffusion of water vapor, *Journal of Physical Chemistry,* vol. 67, no. 1, pp. 126-129, 1963

Cary, J. W., An evaporation experiment and its irreversible thermodynamics, *International Journal of Heat and Mass Transfer,* vol. 7, no. 5, pp. 531-538, 1964

Davis, D. D., Horton, R., Heitman, J. L., and Ren, T, Wettability and hysteresis effects on water sorption in relatively dry soil, *Soil Science Society of America Journal,* vol. 7, no. 6, pp. 1947-1951, 2009

Davis, D. D., Horton, R., Heitman, J. L., and Ren, T, An experimental study of coupled heat and water transfer in wettable and artificially hydrophobized soils, *Soil Science Society of America Journal,* vol. 78, no. 1, pp. 125-132, 2014

Deegan, R. D., Bakajin, O., Dupont, T. F., Huber, G., Nagel, S. R., and Witten, T. A., Contact line deposits in an evaporating drop. *Physical Review E - Statistical Physics, Plasmas, Fluids, and Related Interdisciplinary Topics,* vol. 62, no. (1 B), pp. 756-765, 2000

De Bisschop, F. R. E., and Rigole, W. J. L., A physical model for liquid capillary bridges between adsorptive solid spheres: The nodoid of plateau, *Journal of Colloid and Interface Science,* vol. 88, no. 1, pp. 117-128, 1982

De Vries, D. A., Simultaneous transfer of heat and moisture in porous media. *Eos, Transactions American Geophysical Union,* vol. 39, no. 5, pp. 909-916, 1958

Erbil, H. Y., Evaporation of pure liquid sessile and spherical suspended drops: A review, *Advances in Colloid and Interface Science,* vol. 170, no. 1-2, pp. 67-86, 2012

Fairbrother, R., and Simons, S, The rapture energy of liquid bridges between sphere; the effect of contact angle and separation distance on liquid bridge geometries, *World Congress on Particle Technology 3*, 1998

Farmer, T. P., and Bird, J. C, Asymmetric capillary bridges between contacting spheres, *Journal of Colloid and Interface Science,* vol. 454, pp. 192-199, 2015

Gladkyy, A., and Schwarze, R, Comparison of different capillary bridge models for application in the discrete element method, *Granular Matter,* vol. 16, no. 6, pp. 911-920, 2014

Gleeson, T., Alley, W. M., Allen, D. M., Sophocleous, M. A., Zhou, Y., Taniguchi, M., and VanderSteen, J, Towards sustainable groundwater use: setting long-term goals, backcasting, and managing adaptively, *Groundwater,* vol. 50, no. 1, pp. 19-26, 2012

Haque, M. R., Qu, C., Kinzel, E. C., Betz, A. R., Droplet Growth Dynamics during Atmospheric Condensation on Nanopillar Surfaces, *Journal of Nanoscale Microscale Thermophysical Engineering,* vol. 22, no. 4, pp. 270-295, 2018

Hornbeck, R., and Keskin, P, The historically evolving impact of the ogallala aquifer: Agricultural adaptation to groundwater and drought, *American Economic Journal: Applied Economics,* vol. 6, no. 1, pp. 190-219, 2014

Hu, H., and Larson, R. G., Evaporation of a sessile droplet on a substrate, *Journal of Physical Chemistry B,* vol. 106, no. 6, pp. 1334-1344, 2002

Jury, W. A., and Letey Jr, J., WATER VAPOR MOVEMENT IN SOIL: RECONCILIATION OF THEORY AND EXPERIMENT, *Soil Science Society of America Journal,* vol. 43, no. 5, pp. 823-827, 1979

Keatts, M. I., Daniels, J. L., Langley, W. G., Pando, M. A., and Ogunro, V. O., Apparent contact angle and water entry head measurements for organo-silane modified sand and coal fly ash, *Journal of Geotechnical and Geoenvironmental Engineering,* vol. 144, no. 6, 2018

Lambert, P., Chau, A., Delchambre, A., and Régnier, S., Comparison between two capillary forces models, *Langmuir,* vol. 24, no. 7, pp. 3157-3163, 2008

Lian, G., Thornton, C., and Adams, M. J., A theoretical study of the liquid bridge forces between two rigid spherical bodies, *Journal of Colloid and Interface Science,* vol. 161, no. 1, pp. 138-147, 1993

Nguyen, T. A. H., Nguyen, A. V., Hampton, M. A., Xu, Z. P., Huang, L., and Rudolph, V, Theoretical and experimental analysis of droplet evaporation on solid surfaces, *Chemical Engineering Science,* vol. 69, no. 1, pp. 522-529, 2012

Oki, T., and Kanae, S., Global hydrological cycles and world water resources, *Science,* vol. 313, no. 5790, pp. 1068-1072, 2006

Orejon, D., Sefiane, K., and Shanahan, M. E. R., Stick-slip of evaporating droplets: Substrate hydrophobicity and nanoparticle concentration, *Langmuir,* vol. 27, no. 21, pp. 12834-12843, 2011

Philip, J. R., and De Vries, D. A., Moisture movement in porous materials under temperature gradients, *Eos, Transactions American Geophysical Union,* vol. 38, no. 2, pp. 222-232, 1957

Pietsch, W., and Rumpf, H. Haftkraft, Kapillardruck, Flüssigkeitsvolumen und Grenzwinkel einer Flüssigkeitsbrücke zwischen zwei Kugeln, *Chemie Ingenieur Technik,* vol. 39, no. 15, pp. 885-893, 1967

Pitois, O., Moucheront, P., and Chateau, X., Rupture energy of a pendular liquid bridge, *European Physical Journal B,* vol. 23, no. 1, pp. 79-86, 2001

Rabinovich, Y. I., Esayanur, M. S., and Moudgil, B. M., Capillary forces between two spheres with a fixed volume liquid bridge: Theory and experiment, *Langmuir,* vol. 21, no. 24, pp. 10992-10997, 2005

Rossetti, D., Pepin, X., and Simons, S. J. R., Rupture energy and wetting behavior of pendular liquid bridges in relation to the spherical agglomeration process, *Journal of Colloid and Interface Science,* vol. 261, no. 1, pp. 161-169, 2003

Rynhart, P., McLachlan, R., Jones, J., and McKibbin, R., Solution of the Young-Laplace equation for three particles*, Res. Lett. Inf. Math. Sci.,* vol. 5, pp. 119-127, 2003.

Sáenz, P. J., Wray, A. W., Che, Z., Matar, O. K., Valluri, P., Kim, J., and Sefiane, K., Dynamics and universal scaling law in geometrically-controlled sessile drop evaporation, *Nature Communications,* vol. 8, no. 14783, 2017

Shang, J., Flury, M., Harsh, J. B., and Zollars, R. L., Comparison of different methods to measure contact angles of soil colloids, *Journal of Colloid and Interface Science,* vol. 328, no. 2, pp. 299-307, 2008

Shokri, N., Lehmann, P., and Or, D., Effects of hydrophobic layers on evaporation from porous media, *Geophysical Research Letters,* vol. 35, no. 19, 2008

Singh, S. K., Gogna, M., Muralidhar, K., and Khandekar, S., Combined effect of substrate wettability and thermal properties on evaporation dynamics of a sessile droplet, *Interfacial Phenomena and Heat Transfer,* vol. 5, no. 4, pp. 321-335, 2017

Steward, D. R., Bruss, P. J., Yang, X., Staggenborg, S. A., Welch, S. M., and Apley, M. D., Tapping unsustainable groundwater stores for agricultural production in the High Plains Aquifer of Kansas, projections to 2110, *Proceedings of the National Academy of Sciences*, 201220351. 2013

Steward, D. R., and Allen, A. J., Peak groundwater depletion in the High Plains Aquifer, projections from 1930 to 2110, *Agricultural Water Management,* vol. 170, pp. 36-48, 2016

Suzuki, S., and Ueno, K., Apparent Contact Angle Calculated from a Water Repellent Model with Pinning Effect, *Langmuir: the ACS journal of surfaces and colloids,* vol. 33, no. 1, pp. 138-143. 2017

United Nations, *World population projected to reach 9.8 billion in 2050, and 11.2 billion in 2100,* accessed January 20, 2019, from https://www.un.org/development/desa/en/news/population/world-population-prospects-2017.html , 2017

Wang, J. P., Gallo, E., François, B., Gabrieli, F., and Lambert, P., Capillary force and rupture of funicular liquid bridges between three spherical bodies, *Powder Technology,* vol. 305, pp. 89-98, 2017

Weigert, T., and Ripperger, S., Calculation of the liquid bridge volume and bulk saturation from the half-filling angle, *Particle and Particle Systems Characterization,* vol. 16, no. 5, pp. 238-242, 1999

Willett, C. D., Adams, M. J., Johnson, S. A., and Seville, J. P. K., Capillary bridges between two spherical bodies, *Langmui,* vol. 16, no. 24, pp. 9396-9405, 2000

Wise, L. A., drying shame: With the Ogallala Aquifer in peril, the days of irrigation for western Kansas seem numbered, *The Kansas City Star*, 2015

Zhu, H. P., Zhou, Z. Y., Yang, R. Y., and Yu, A. B., Discrete particle simulation of particulate systems: Theoretical developments. *Chemical Engineering Science,* vol. 62, no. 13, pp. 3378-3396, 2007

Figure Captions

Figure 1: Evaporation of sessile 4-μL water droplet from a simulated soil pore created with three hydrophilic glass or hydrophobic PTFE beads

Figure 2: Distances between (a) 3 glass beads (a=~3.1 mm), (b) 3 Teflon beads (a=~3.1 mm), (c) 3 glass beads (a=~2.7mm, b=~2.8 mm), and (d) 3 Teflon beads (a=~2.7mm, b=~2.8 mm)

Figure 3: Goniometer images of sessile water droplets on a) flat glass plate, b) flat Teflon plate, c) glass beads (center-to-center spacing approximately one diameter), d) Teflon beads (center-to-center spacing approximately one diameter) and side-view camera images of water droplets on e) glass and f) Teflon pores in the asymmetric spacing

Figure 4: Projected area of whole droplet. The plot represents the change in projected area during evaporation and figures a_1, b_1, c_1, d_1 are the initial and a_2, b_2, c_2, d_2 are the final projected areas in glass and Teflon for symmetric and asymmetric combination respectively.

Error! Reference source not found.

Figure 6: Variation of radius of curvature of liquid island with time. glass beads at (a_1) t= 18 minutes and (a_2) t = 30 minutes and in Teflon beads at (b_1) t = 28 minutes and (b_2) t = 43 minutes (symmetric combination). Glass beads at (c_1) t = 34 minutes and (c_2) t= 42 minutes, Teflon beads at (d_1) t = 42 minutes and (d_2) t = 52 minutes (asymmetric combination)

Figure 7: Change of wetted length of whole droplet. a_1, b_1, c_1 and d_1 represent the initial wetted length, a_2, b_2, c_2 and d_2 represent the wetted length at 14^{th} minutes and a_3, b_3, c_3 and d_3 represent the wetted length just before the breakup of whole droplet in Glass and Teflon where a and b represent the symmetric and c and d asymmetric combination respectively

Figure 8: Change of Wetted length of liquid island

Figure 9: Liquid island between two beads

Figure 10: Change of volume of liquid island with time

Figure 11: Variation of contact angle with volume

Figure 12: Variation of rupture strength/capillary force with time

Figures

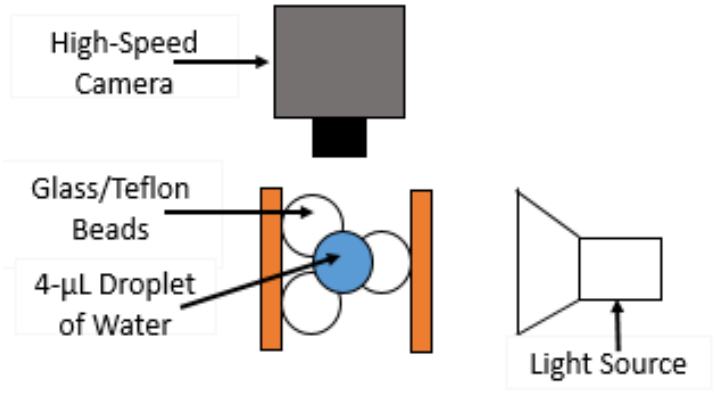

Figure 1: Evaporation of sessile 4-µL water droplet from a simulated soil pore created with three hydrophilic glass or hydrophobic PTFE beads

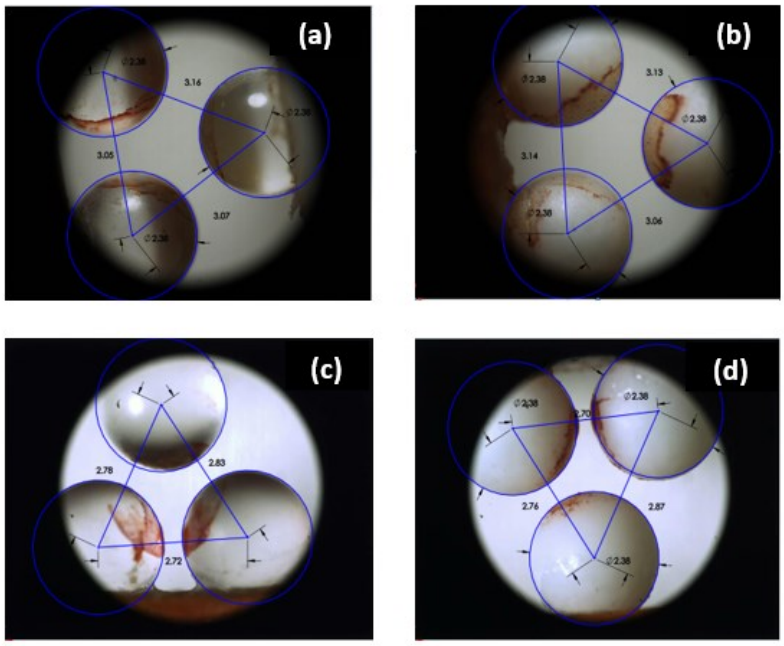

Figure 2: Distances between (a) 3 glass beads (a=~3.1 mm), (b) 3 Teflon beads (a=~3.1 mm), (c) 3 glass beads (a=~2.7mm, b=~2.8 mm), and (d) 3 Teflon beads (a=~2.7mm, b=~2.8 mm)

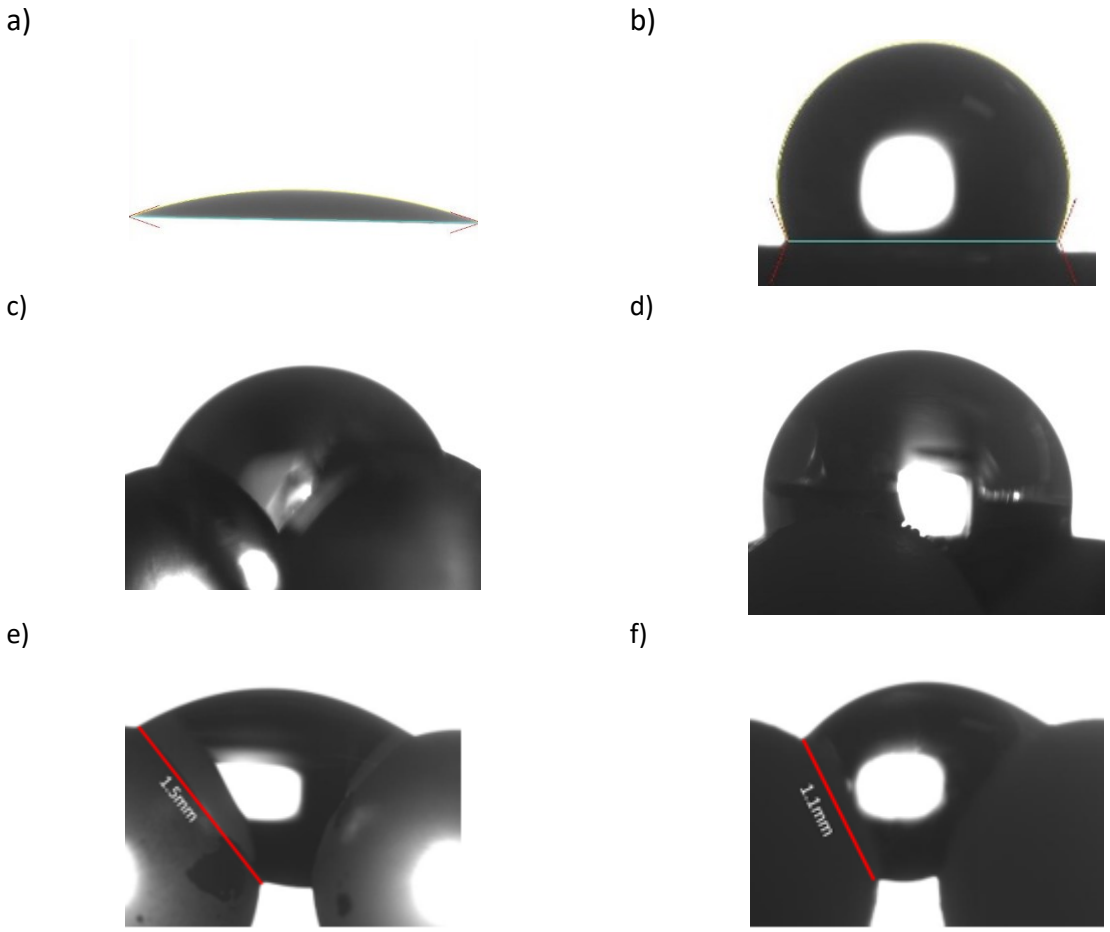

Figure 3: Goniometer images of sessile water droplets on a) flat glass plate, b) flat Teflon plate, c) glass beads (center-to-center spacing approximately one diameter), d) Teflon beads (center-to-center spacing approximately one diameter) and side-view camera images of water droplets on e) glass and f) Teflon pores in the asymmetric spacing

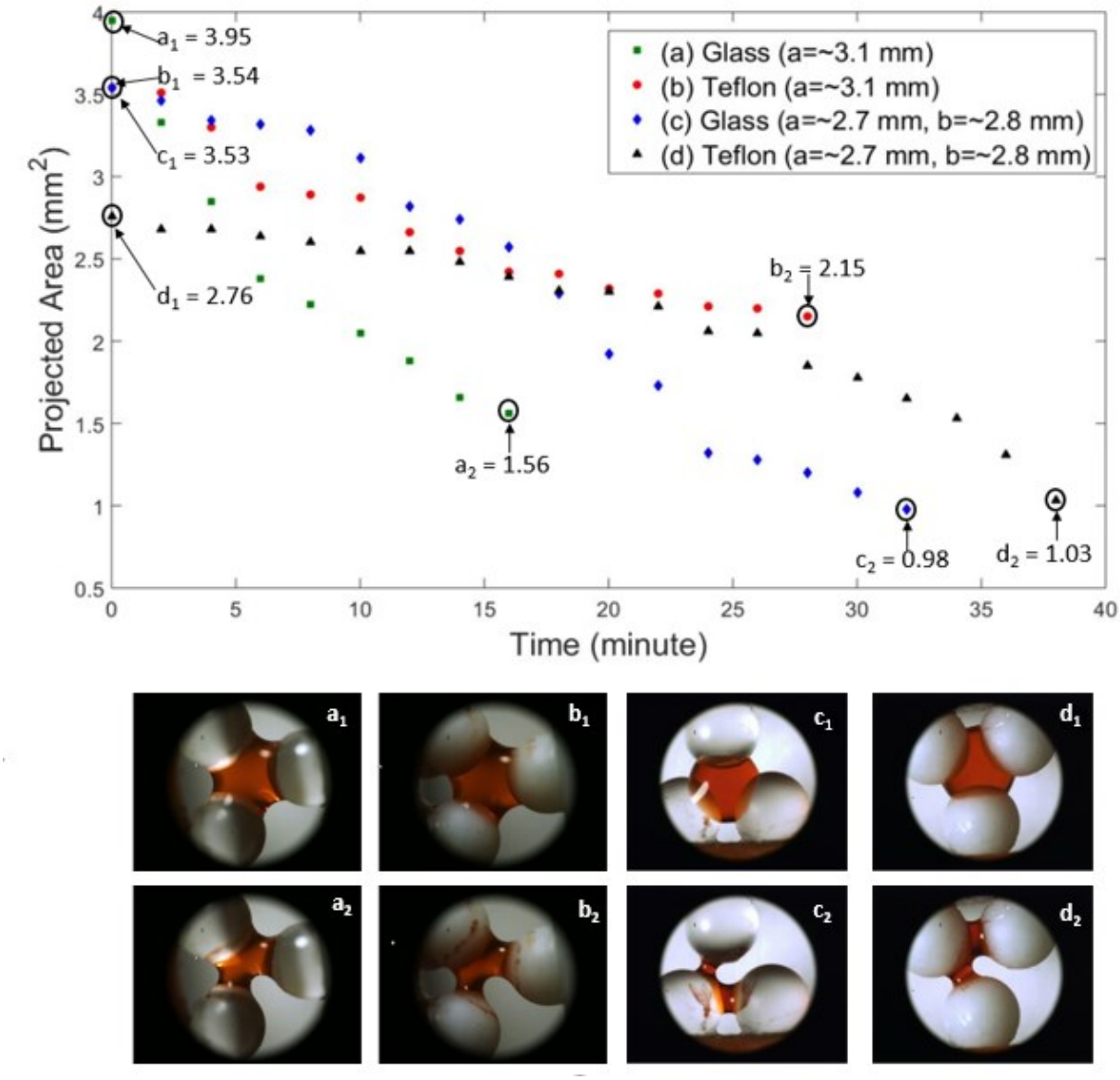

Figure 4: Projected area of whole droplet. The plot represents the change in projected area during evaporation and figures a1, b1, c1, d1 are the initial and a2, b2, c2, d2 are the final projected areas in glass and Teflon for symmetric and asymmetric combination respectively.

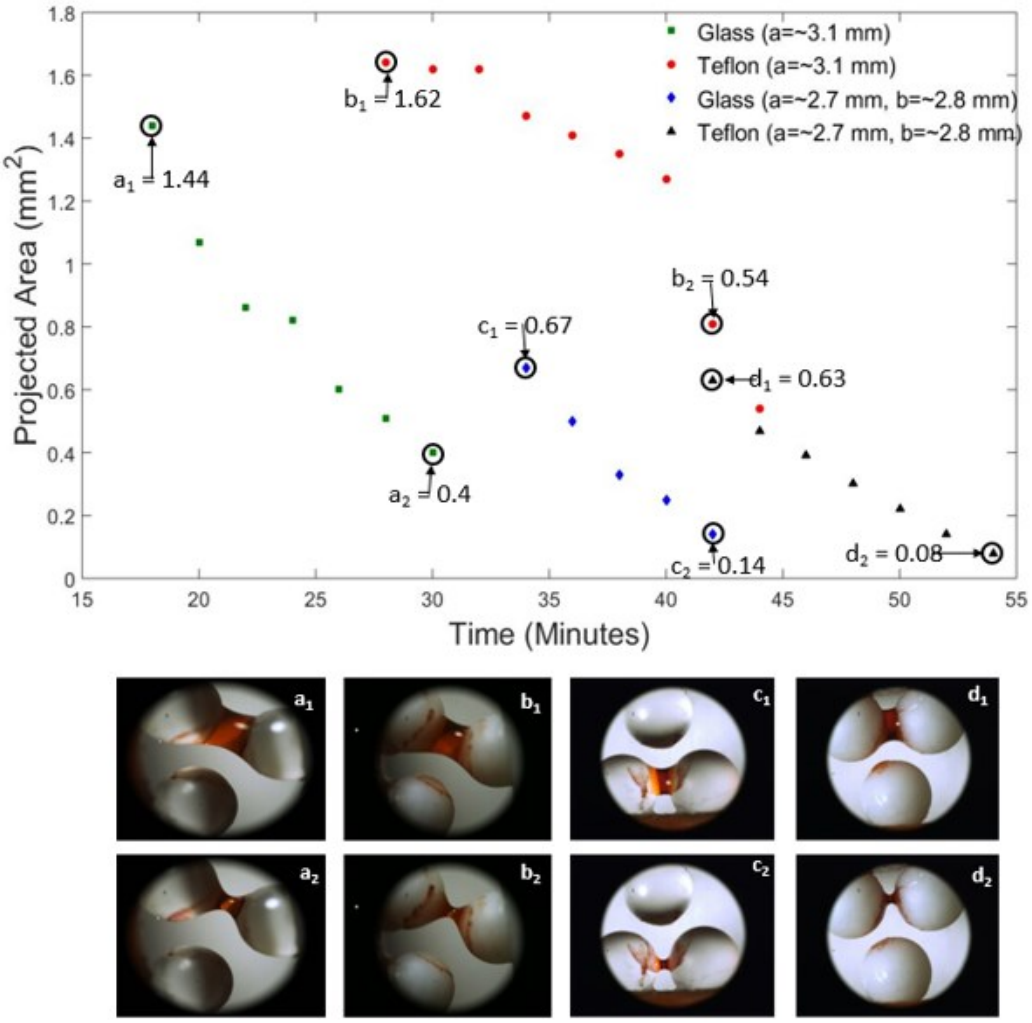

Figure 5: Projected area evolutions of liquid islands, for liquid island formation (a_1, b_1, c_1, d_1) and immediately preceding liquid island breakup (a_2, b_2, c_2, d_2) for glass and Teflon beads

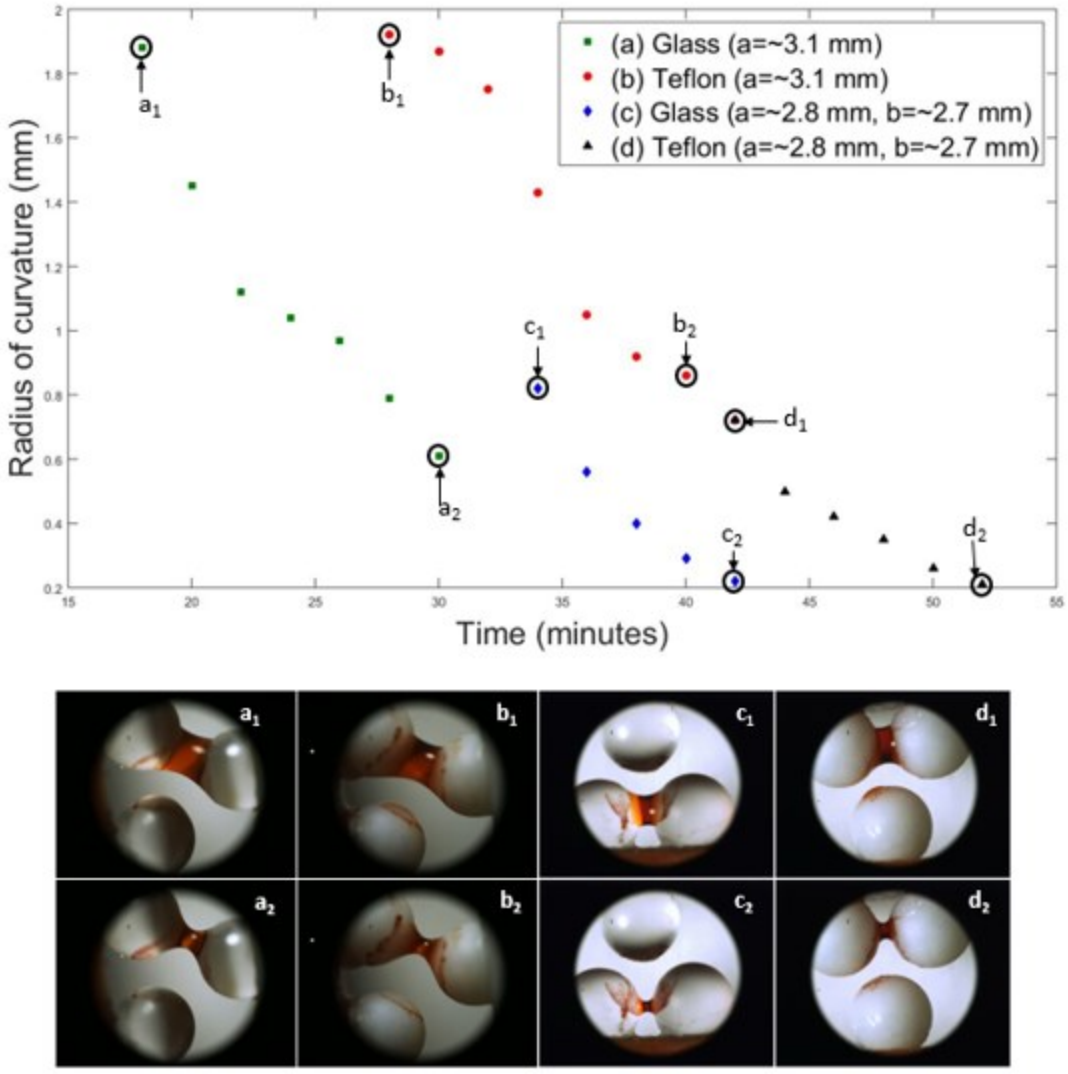

Error! Reference source not found.

Figure 6: Variation of radius of curvature of liquid island with time. glass beads at (a1) t= 18 minutes and (a2) t = 30 minutes and in Teflon beads at (b1) t = 28 minutes and (b2) t = 43 minutes (symmetric combination). Glass beads at (c1) t = 34 minutes and (c2) t= 42 minutes, Teflon beads at (d1) t = 42 minutes and (d2) t = 52 minutes (asymmetric combination)

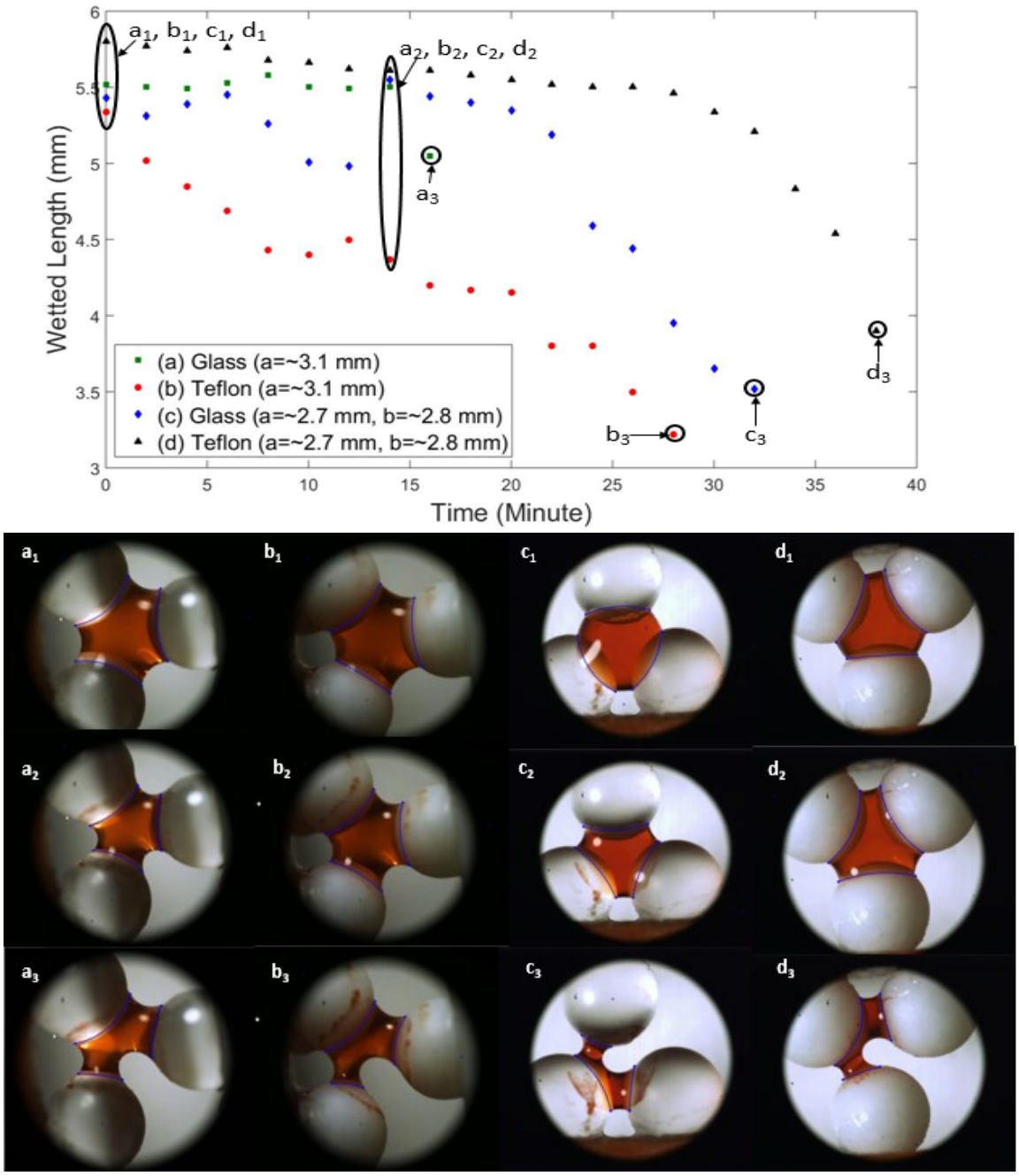

Figure 7: Change of wetted length of whole droplet. a1, b1, c1 and d1 represent the initial wetted length, a2, b2, c2 and d2 represent the wetted length at 14th minutes and a3, b3, c3 and d3 represent the wetted length just before the breakup of whole droplet in Glass and Teflon where a and b represent the symmetric and c and d asymmetric combination respectively

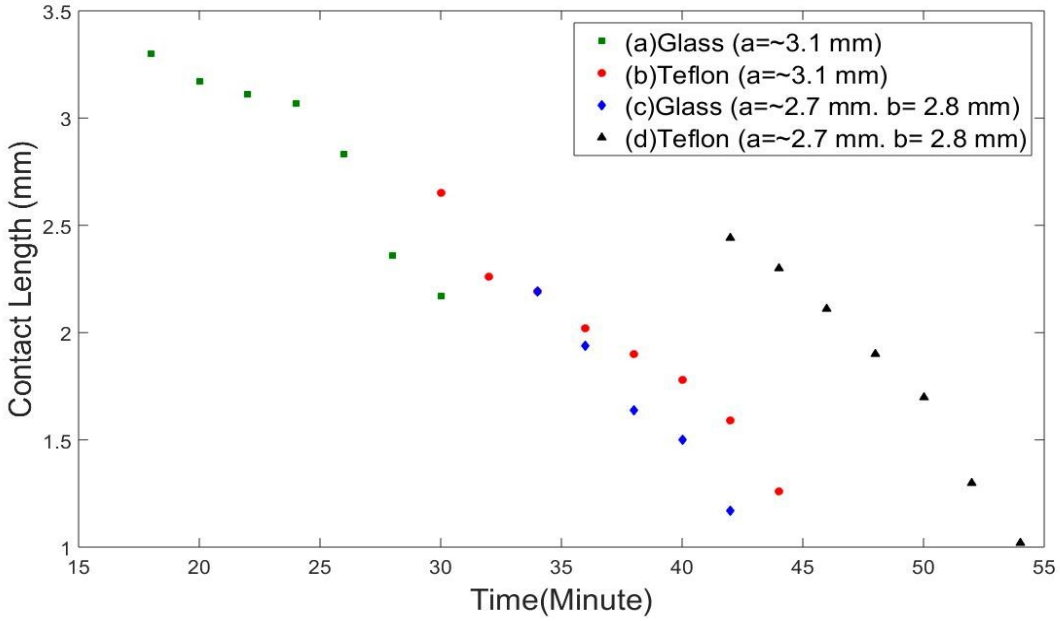

Figure 8: Change of Wetted length of liquid islands

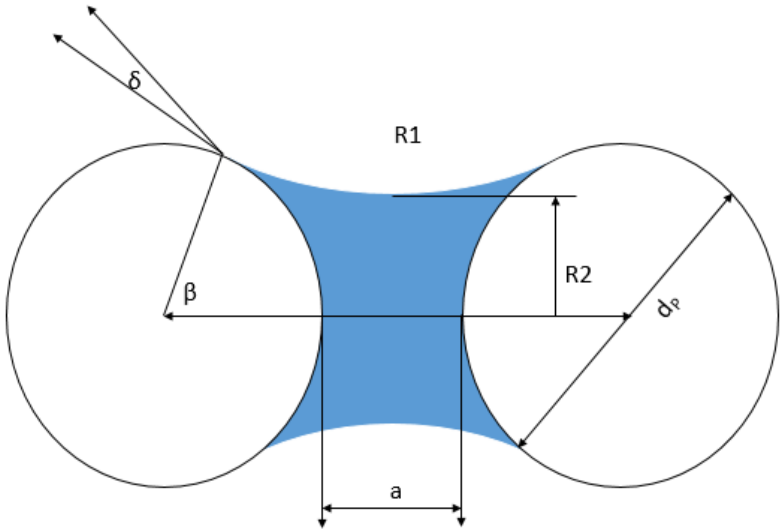

Figure 9: Liquid island between two beads

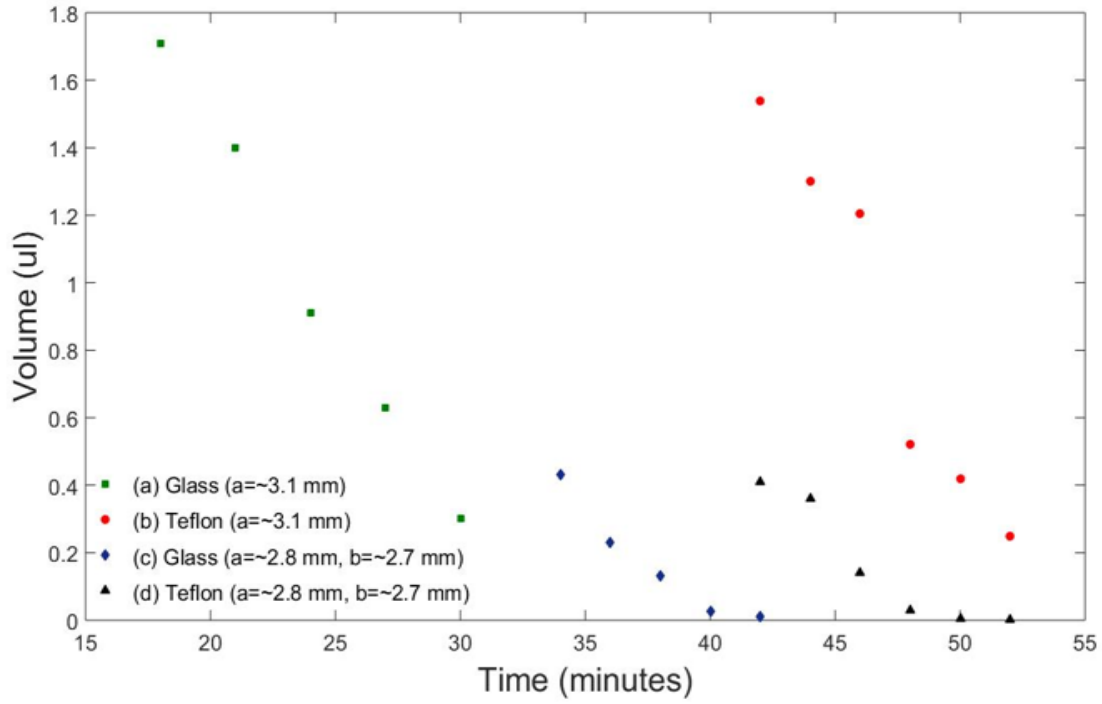

Figure 10: Change of volume of liquid island with time

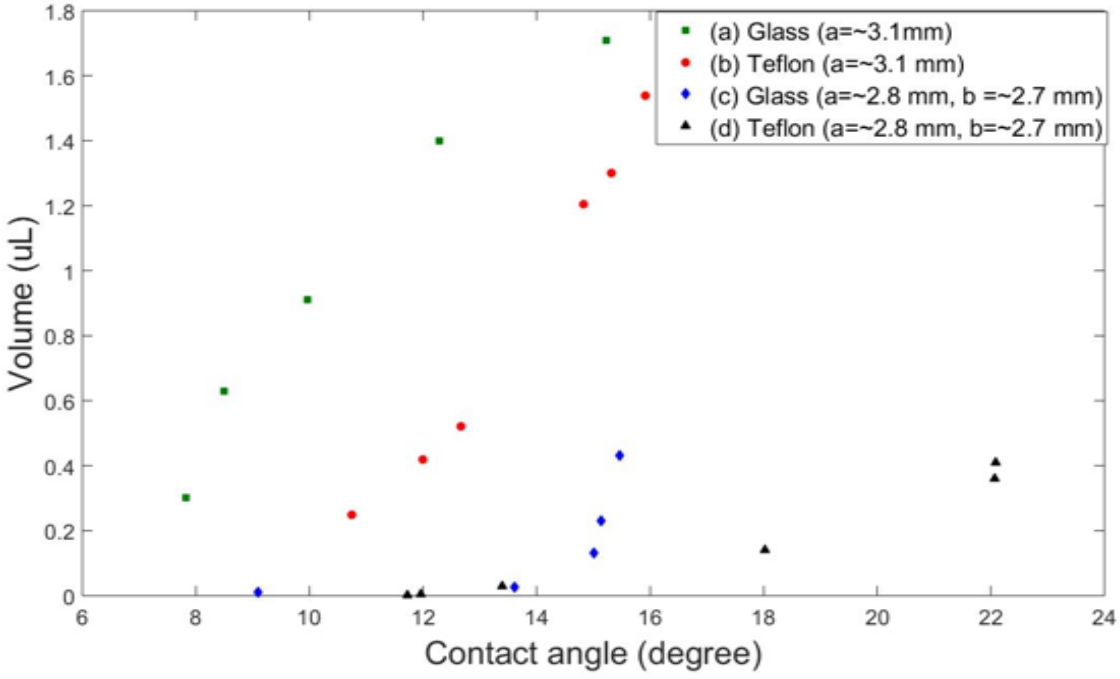

Figure 11: Variation of contact angle with volume

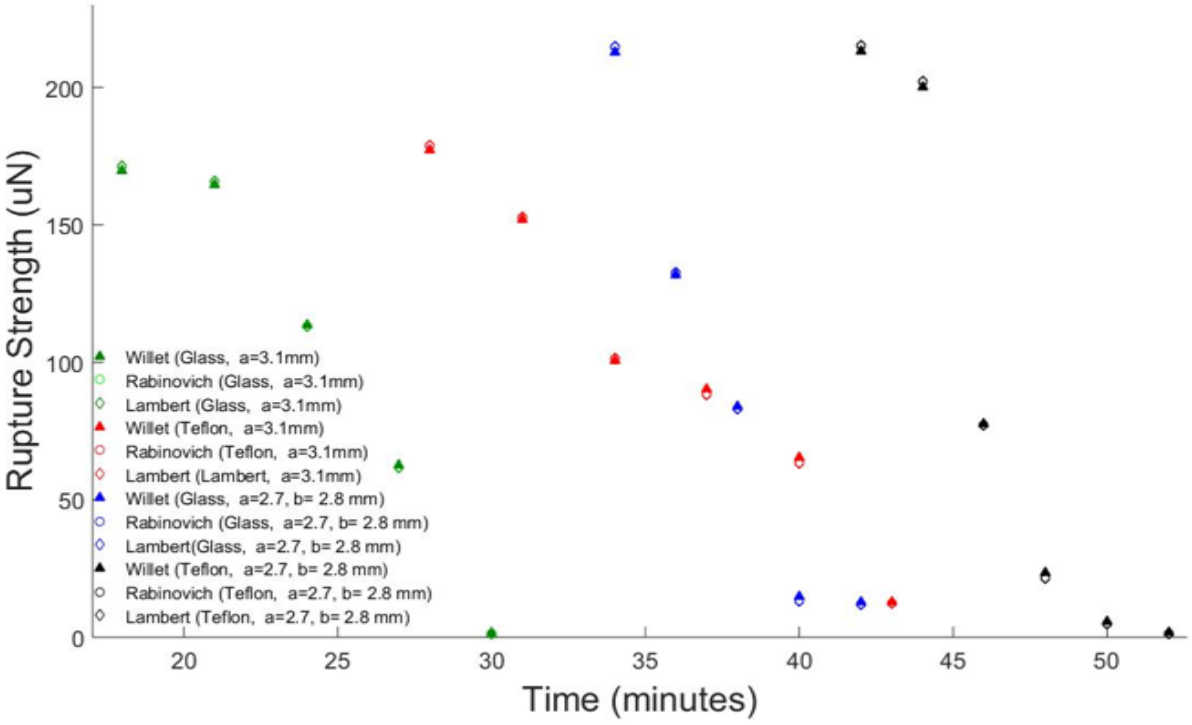

Figure 12: Variation of rupture strength/capillary force with time

List of Tables

Tables

Table 1: Evaporation time for the configurations of three glass and Teflon beads

3 Glass (a=~3.1 mm)		**3 Teflon(a=~3.1 mm)**		**3 Glass(a=~2.7 mm, b=~2.8 mm)**		**3 Teflon(a=~2.7 mm, b=~2.8 mm)**	
Replication Number	Evaporation Time (Minutes)	Replication Number	Evaporation Time (Minutes)	Replication Number	Evaporation Time (Minutes)	Replication Number	Evaporation Time (Minutes)
1	32	1	38	1	42	1	55
2	33	2	44	2	43	2	56
3	35	3	43	3	39	3	53
4	34	4	41	4	41	4	54
Average Time: **34 minutes**		Average Time: **42 minutes**		Average Time: **42 minutes**		Average time : **55 minutes**	

Table 2: Average time for liquid island formation

Combination	Liquid Island Formation time (minutes)
Glass (a=~3.1 mm)	19 minutes
Teflon (a=~3.1 mm)	28 minutes
Glass (a=~2.8 mm, b=~2.7 mm)	35 minutes
Teflon (a=~2.8 mm, b=~2.7 mm)	43 minutes

Table 3: Uncertainty analysis

	Contact Angle, δ (degree)				Principal Radius of Curvature,R_1 (mm)				Principal Radius of Curvature,R_2 (mm)			
1	15.23	12.28	9.97	8.5	1.88	1.3	1.04	0.83	0.7	0.63	0.53	0.45
2	15.3	12.4	9.9	8.33	1.85	1.33	1.02	0.82	0.71	0.62	0.52	0.44
3	15.28	12.36	9.85	8.36	1.88	1.35	1.03	0.82	0.7	0.62	0.53	0.44
4	15.32	12.44	9.92	8.42	1.87	1.33	1.04	0.81	0.71	0.63	0.52	0.45
Uncertainties	0.5%	1.3%	1.21%	1.67%	1.6%	1.5%	1.9%	1.22%	1.39%	1.59%	1.89%	2.22%